



A Theranostic Agent Combining a Two-Photon-Absorbing Photosensitizer for Photodynamic Therapy and a Gadolinium(III) Complex for MRI Detection

Julie Schmitt, Valérie Heitz, Angélique Sour, Frédéric Bolze, Pascal Kessler, Lucia Flamigni, Barbara Ventura, Célia S. Bonnet, Éva Tóth

► To cite this version:

Julie Schmitt, Valérie Heitz, Angélique Sour, Frédéric Bolze, Pascal Kessler, et al.. A Theranostic Agent Combining a Two-Photon-Absorbing Photosensitizer for Photodynamic Therapy and a Gadolinium(III) Complex for MRI Detection. *Chemistry - A European Journal*, 2016, 22 (8), pp.2775-2786. 10.1002/chem.201503433 . hal-01407691

HAL Id: hal-01407691

<https://hal.science/hal-01407691>

Submitted on 31 Jan 2022

HAL is a multi-disciplinary open access archive for the deposit and dissemination of scientific research documents, whether they are published or not. The documents may come from teaching and research institutions in France or abroad, or from public or private research centers.

L'archive ouverte pluridisciplinaire **HAL**, est destinée au dépôt et à la diffusion de documents scientifiques de niveau recherche, publiés ou non, émanant des établissements d'enseignement et de recherche français ou étrangers, des laboratoires publics ou privés.

■ Photodynamic Therapy

A Theranostic Agent Combining a Two-Photon-Absorbing Photosensitizer for Photodynamic Therapy and a Gadolinium(III) Complex for MRI Detection

Julie Schmitt,^[a] Valérie Heitz,^{*[a]} Angélique Sour,^[a] Frédéric Bolze,^{*[b]} Pascal Kessler,^[c] Lucia Flamigni,^[d] Barbara Ventura,^{*[d]} Célia S. Bonnet,^[e] and Éva Tóth^{*[e]}

Abstract: ■■■ please provide academic titles (Prof., Prof. Dr., Dr.) for the authors ■■■ The convergent synthesis and characterization of a potential theranostic agent, [DPP-ZnP-GdDOTA][−], which combines a diketopyrrolopyrrole-porphyrin component DPP-ZnP as a two-photon photosensitizer for photodynamic therapy (PDT) with a gadolinium(III) DOTA complex as a magnetic resonance imaging probe, is presented. [DPP-ZnP-GdDOTA][−] has a remarkably high longitudinal water proton relaxivity (19.94 mM^{−1}s^{−1} at 20 MHz and 25 °C) for a monohydrated molecular system of this size. The nuclear magnetic relaxation dispersion (NMRD) profile is characteristic of slow rotation, related to the extended and

rigid aromatic units integrated in the molecule and to self-aggregation occurring in aqueous solution. The two-photon properties were examined and large two-photon absorption cross-sections around 1000 GM were determined between 910 and 940 nm in dichloromethane (DCM) with 1% pyridine and in DMSO. Furthermore, the new conjugate was able to generate singlet oxygen, with quantum yield of 0.42 and 0.68 in DCM with 1% pyridine and DMSO, respectively. Cellular studies were also performed. The [DPP-ZnP-GdDOTA][−] conjugate demonstrated low dark toxicity and was able to induce high one-photon and moderate two-photon phototoxicity on cancer cells.

Introduction

The combination of therapy and diagnosis has led to a new field of research named theranostics, the aim of which is to develop mild, efficient, and personalized treatments. Associating an imaging modality to a therapeutic agent offers a promising way to improve treatment by monitoring in vivo the delivery and/or the effect of a drug. Several strategies have been pro-

posed to obtain theranostic agents based on molecular systems as well as on nanoparticles.^[1]

As a diagnostic tool, magnetic resonance imaging (MRI) is widely used in medicine. It is a non-invasive modality, which provides images with excellent anatomical and temporal resolution. A disadvantage of this technique, however, is its low sensitivity requiring high concentrations of the contrast agents to be injected.^[2] Commercial contrast agents, based on paramagnetic gadolinium complexes, are extracellular and have low MRI efficiency. Their relaxivities, which measure the paramagnetic enhancement of the longitudinal water proton relaxation rate, are only in the order of 4–5 mM^{−1}s^{−1}.^[3] These values could be significantly improved by optimizing the parameters that influence relaxivity of the Gd^{III} complexes, such as the hydration number, the water exchange rate or the rotational dynamics, by structural modifications.^[4]

Photodynamic therapy (PDT) is a minimally invasive therapy, based on the localized light activation of a photosensitizer that reacts with surrounding oxygen to produce singlet oxygen or cytotoxic oxygen reactive species^[5] produced by energy or electron transfer from the triplet excited state of the photosensitizer. Although it is frequently applied to various skin diseases, age-related macular degeneration and cancerous tumors, it suffers from several limitations. These involve low tissue penetration of the visible light currently used in PDT, and photo-damage induced by the excitation light outside the therapeutic window (between 700 and 1000 nm), which is absorbed by various endogenous chromophores. Recently, PDT based on

[a] J. Schmitt, V. Heitz, A. Sour
Laboratoire de Synthèse des Assemblages Moléculaires Multifonctionnels,
Institut de Chimie de Strasbourg, CNRS/UMR 7177, Université de Strasbourg,
4, rue Blaise Pascal, 67000 Strasbourg (France)
E-mail: v.heitz@unistra.fr

[b] F. Bolze
CAMB, UMR 7199, Uds/CNRS, Faculté de Pharmacie
Université de Strasbourg, 74 route du Rhin, 67401 Illkirch (France)
E-mail: frederic.bolze@unistra.fr

[c] P. Kessler
Institute of Genetics and Molecular and Cellular Biology
1, rue Laurent Fries, 67404 Illkirch (France)

[d] L. Flamigni, B. Ventura
Istituto ISOF-CNR, Via P. Gobetti 101, 40129 Bologna (Italy)
E-mail: barbara.ventura@isof.cnr.it

[e] C. S. Bonnet, É. Tóth
Centre de Biophysique Moléculaire UPR4301, CNRS, Université d'Orléans,
rue Charles Sadron, 45071 Orléans (France)
E-mail: eva.jakabtoth@cnrs-orleans.fr

Supporting information for this article is available on the WWW under
<http://dx.doi.org/10.1002/chem.201503433>.

two-photon excitation of a photosensitizer performed in the near infrared region with short focalized laser pulses has proven to be a promising approach to circumvent those limitations.^[6]

The design of theranostic agents that combine MRI detection capabilities with two-photon sensitization ability for PDT is a further step towards a better control of this mild and efficient therapy.^[7] The most obvious benefit of such agents is indeed to monitor the delivery of the photosensitizer to the site of interest, to have a precise localization of the damaged area and to treat it with high spatial resolution by means of the combined imaging and therapeutic functions. Ideally, the conjugation of the MRI contrast agent to a porphyrin derivative, known to preferentially accumulate in tumor tissues, should not substantially change the biodistribution and the therapeutic agent will act as a vehicle to deliver the MRI agent to the area of the treatment. On the other hand, the chemical association of the photosensitizer to the MRI probe can also improve its relaxation properties. The increased size of the theranostic system as compared to the contrast agent alone will enhance its relaxivity by slowing down the rotational dynamics of the Gd^{III} center, provided that the whole molecule keeps a low inner flexibility.^[3] Moreover, the photosensitizer can benefit from the linkage with the Gd^{III} ion, which could promote intersystem crossing to the triplet state by heavy atom effect^[8] and enhance the triplet yield. Finally, as each component (the Gd^{III} complex and the photosensitizer) retains its activity within the conjugate without a need of in vivo cleavage, the real-time monitoring of not only the delivery but also the excretion of the theranostic agent becomes possible.

Few molecular systems consisting of Gd^{III} complexes associated to a porphyrin derivative used as a one-photon photosensitizer for PDT have been reported to behave both as MRI contrast agents and singlet oxygen generators.^[9] In those examples, the relaxivity of the contrast agent constructed on a porphyrin core was greatly affected by the size and flexibility of the whole molecule. Various strategies have also been proposed to assemble high concentrations of the MRI probe and of the photosensitizer in a nanoparticle.^[10] However, their random proportion renders the pharmacokinetics of such systems difficult to predict. For the molecular PDT-MRI conjugate systems reported so far, the optimization of the PDT sensitizer component remains to be done, in particular in terms of lowering the excitation energy close to the therapeutic window (700–1000 nm) to achieve higher penetration depth in tissues. This can be pursued mainly by two approaches: 1) by lowering the HOMO–LUMO gap of the sensitizer through an appropriate chemical modification, or 2) by using a sensitizer with high two-photon absorption (TPA) cross-section in the therapeutic window. The application of a two-photon sensitizer implies also the advantages inherent to the TPA phenomenon, that is, increased spatial resolution of the treatment and decreased photodamage of the surrounding tissues.^[6g]

Following the second strategy, we herein describe the convergent synthesis of the theranostic agent [DPP-ZnP-GdDOTA][−] that associates a diketopyrrolopyrrole–zinc(II) porphyrin component as two-photon absorbing photosensitizer for PDT with

GdDOTA as MRI probe (H₄DOTA = 1,4,7,10-tetraazacyclododecane-1,4,7,10-tetraacetic acid). We have evaluated the two-photon absorption properties, the singlet oxygen generation as well as the relaxivity of the new conjugate in solution. Cell penetration and two-photon excitation experiments in cells have been carried out to assess its potential as a near-IR two-photon PDT photosensitizer.

Results and Discussion

The design of the theranostic system [DPP-ZnP-GdDOTA][−] was based on a convergent synthesis that couples in the last step two well-defined components, a diketopyrrolopyrrole–zinc(II)-porphyrin component, DPP-ZnP-NH₂, decorated with hydrophilic oligoethylene glycol chains, and an anionic [GdDOTA-GA]^{2−} complex, which provides sufficient water solubility to the final compound for biological applications (Figure 1). The use of a diketopyrrolopyrrole–porphyrin conjugate as a component of the theranostic agent was motivated by our recent studies on a related conjugate, DPP-ZnP-TIPS. This robust dye has a large delocalized π -system and showed high TPA cross-section in the near-IR.^[11] Furthermore, it generated efficiently singlet oxygen in solution, penetrated readily in cells, and exhibited high two-photon induced phototoxicity on HeLa cell cultures.

The final hetero-dinuclear [DPP-ZnP-GdDOTA][−] complex, incorporating a Zn^{II} in the porphyrin and a Gd^{III} in the DOTA chelate, could be conceived from the pre-metallated macrocyclic ligands by a careful choice of the reaction conditions to avoid demetalation of these acid-sensitive complexes. An amide bond formation in mild conditions was able to satisfy these requirements. The DPP-ZnP-NH₂ component can be readily obtained from DPP-ZnP-TIPS (Figure 2).^[11] The [GdDOTAGA]^{2−} precursor contains a DOTA-like ligand, a common macrocyclic chelator for gadolinium(III)-based contrast agents that provides high thermodynamic stability, kinetic inertness, and fast water exchange.^[3] In H₅DOTAGA, one of the acetate pendant arms is functionalized with an additional carboxylic acid. Gd^{III} complexation of [DOTAGA]^{5−} involves four carboxylates and the remaining carboxylate of [GdDOTAGA]^{2−} allows further reaction without using a protection/deprotection step.^[12] The [YDOTA-GA]^{2−} complex was also synthesized and used to prepare the [DPP-ZnP-YDOTA][−] conjugate, as the diamagnetic analogue of the desired paramagnetic [DPP-ZnP-GdDOTA][−] molecule (Figure 2).

The DPP-ZnP-NH₂ component was obtained in two steps from DPP-ZnP-TIPS. After classical cleavage of the triisopropyl silyl group using TBAF, the air-sensitive intermediate DPP-ZnP-H was reacted with the *tert*-butoxycarbonyl (Boc)-protected 3-iodobenzylamine^[13] under standard Sonogashira cross-coupling reaction conditions. Purifications with silica gel chromatography and size-exclusion column chromatography led to DPP-ZnP-NHBoc in 42% yield. Removal of the Boc-protecting group using trifluoroacetic acid led to partial demetalation of the zinc(II) porphyrin, which was remetalated with Zn(OAc)₂·2H₂O to afford DPP-ZnP-NH₂ in almost quantitative yield.

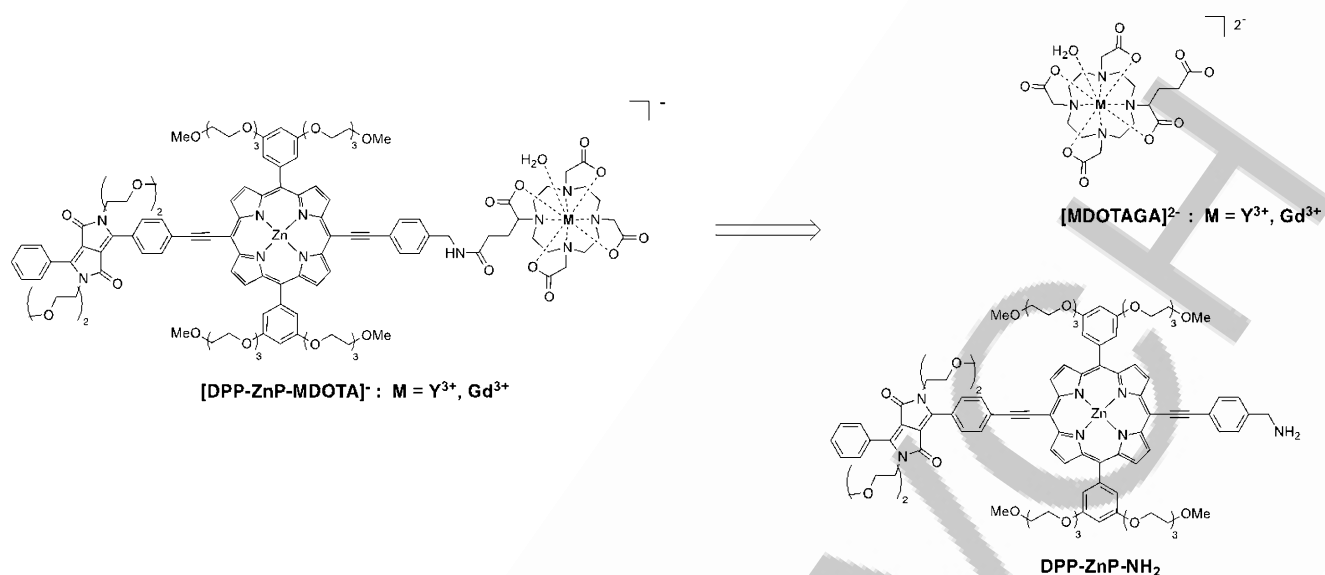


Figure 1. Synthetic strategy to prepare the theranostic system $[\text{DPP-ZnP-GdDOTA}]^{2-}$ from two components, DPP-ZnP-NH_2 and $[\text{GdDOTAGA}]^{2-}$. The related diamagnetic complex $[\text{DPP-ZnP-YDOTA}]^-$ and its precursors are also represented.

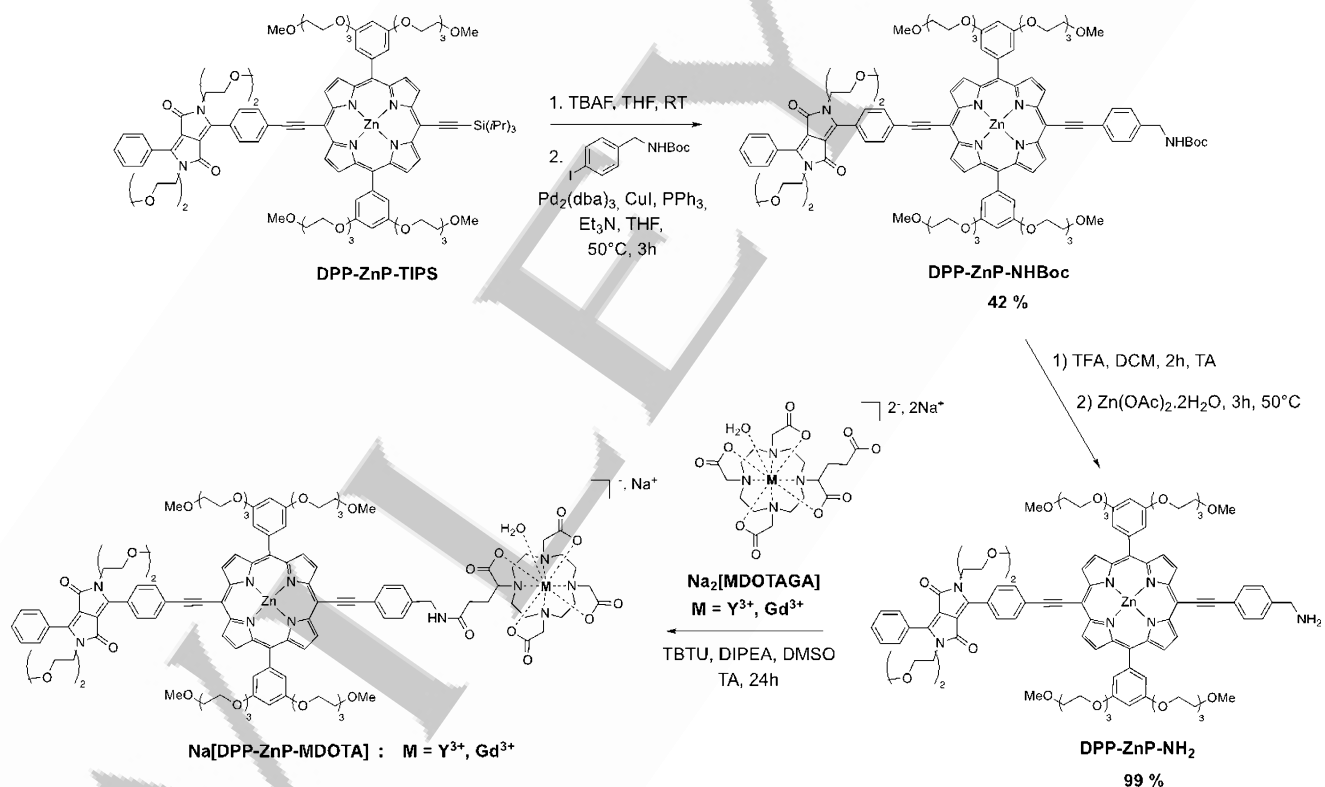


Figure 2. Synthesis of $\text{Na}[\text{DPP-ZnP-MDOTA}]$, $M = \text{Y}^{\text{III}}$ or Gd^{III} .

The complexation of DOTAGA anhydride with GdCl_3 at neutral pH adjusted with an aqueous sodium hydroxide solution gave the complex $\text{Na}_2[\text{GdDOTAGA}]$ as reported.^[12] The amide coupling reaction leading to the final $[\text{DPP-ZnP-GdDOTA}]^{2-}$ molecule was performed by using the sodium salt of the $[\text{GdDO-}$

$\text{TAGA}]^{2-}$ complex, dissolved in DMSO at 65°C before addition of the activating agent *O*-(benzotriazol-1-yl)-*N,N,N',N'*-tetramethyluronium (*N*-TBTU) tetrafluoroborate, and the base *N,N*-diisopropylethylamine (DIPEA). Then a DMSO solution of DPP-ZnP-NH_2 was added dropwise and the reaction mixture was

stirred overnight at room temperature. Size-exclusion column chromatography allowed the removal of the coupling agents and unreacted starting porphyrin from the crude mixture.

The delicate purification of the final molecule was achieved by size-exclusion column chromatography followed by preparative TLC using DCM/MeOH/NH₄OH 80:15:5 as eluent to afford the sodium salt Na[DPP-ZnP-GdDOTA] in 52% yield. The compound was characterized by high-resolution mass spectrometry. The isotopic profile of the molecular ionic species [M + 2Na]⁺, detected at 2470.8131, was in accordance with the calculated one (Supporting Information, Figure S12). The related diamagnetic yttrium(III) complex Na[DPP-ZnP-YDOTA] obtained by reacting [YDOTAGA]²⁻ with DPP-ZnP-NH₂ in similar reaction conditions as for [DPP-ZnP-GdDOTA]⁻ was further characterized with 1D and 2D ¹H NMR spectroscopy in [D₆]DMSO (Supporting Information, Figure S9 and S10).

Relaxivity measurements

To characterize the relaxation efficiency of the theranostic agent [DPP-ZnP-GdDOTA]⁻, nuclear magnetic relaxation dispersion (NMRD) profiles were recorded in water at two different temperatures in the field range of 10 kHz–600 MHz (Figure 3). Some relaxivity data were also obtained in an aqueous solution containing 1% DMSO and were identical to those in water. Likewise, the relaxivities in the presence of 50 mM NaCl were very similar to those measured in H₂O alone (Supporting Information, Figure S14).

The most important parameters that influence relaxivity are the number of water molecules directly coordinated to the Gd^{III} (*q*), their exchange rate with the bulk water (*k_{ex}*), the rotational correlation time of the complex (*τ_R*), and the parameters characterizing electron spin relaxation (*τ_v* and *Δ*²). These parameters govern relaxivity via the Solomon–Bloembergen–Morgan (SBM) theory of paramagnetic relaxation.^[3] We assume that the [DPP-ZnP-GdDOTA]⁻ complex has one inner-sphere

water molecule, analogously to GdDOTA and all similar DOTA derivatives.^[3]

The relaxivity obtained for [DPP-ZnP-GdDOTA]⁻, *r*₁ = 19.94 mM⁻¹s⁻¹ (20 MHz, 25 °C), is remarkably high for a molecular system of this size (MW = 2.4 kDa) incorporating one monohydrated GdDOTA complex. It is only slightly lower than the relaxivity of P760 (*r*₁ ≈ 25 s⁻¹mm⁻¹ between 20 and 60 MHz) with an approximately double molecular weight (MW = 5.3 kDa), which was previously developed as a low diffusion, fast clearance blood pool agent.^[14] In P760, a GdDOTA core is decorated with four large (though not rigid) hydrophilic arms, thus the Gd^{III} is in the barycenter of the molecule and takes full advantage of the slow rotation of the entire system. The relaxivity of [DPP-ZnP-GdDOTA]⁻ is in the same order of magnitude as those reported for various nanosized objects such as MOFs,^[15] polyrotaxanes,^[16] micelles,^[17] and slightly lower than that of optimized gold nanoparticles.^[18] The relaxivity profiles display a high field peak with a maximum at around 20 MHz, which is characteristic of slow rotation (Figure 3). Such slow rotation is the result of the large size of our molecule integrating extended and rigid aromatic systems. Furthermore, a self-aggregation phenomenon occurring in aqueous solution is likely to further contribute to slow rotation. Indeed, self-aggregation is postulated on the basis of the photophysical properties of the conjugate in water (see below). The dilution of the circa 1 mM solution by a factor of two did not have detectable effect on the relaxivity. Water soluble tri- or tetra-anionic porphyrins are known to aggregate spontaneously^[19] and in the present [DPP-ZnP-GdDOTA]⁻ system, the large extended *π*-conjugate system over the diketopyrrolopyrrole–zinc(II)porphyrin conjugate might favor intermolecular *π*–*π* interactions. Self-aggregation resulting in high relaxivities has been often observed for medium-size systems consisting of several Gd^{III} complexes linked to an aromatic core.^[20] Nevertheless, despite the large size and the aggregation of [DPP-ZnP-GdDOTA]⁻, the relaxivity is still limited by rotation and not by slow water exchange, as evidenced by the temperature dependency of the NMRD curves (the relaxivity decreases with increasing temperature).

To gain insight into the rotational dynamics of the system, the microscopic parameters characterizing rotation were assessed by fitting the experimental relaxivity data to the SBM theory. To take into account internal dynamics, we incorporated in the fit the Lipari–Szabo treatment often used to describe rotational motion of slow (ns) tumbling species.^[21] In this approach, the dipolar interactions between the Gd^{III} electron spin and the water proton that generate the relaxation are influenced by both fast local rotational motion of the Gd³⁺–water proton axis, characterized by the correlation time *τ_{RL}*, and a slower, global motion (characterized by *τ_{RG}*) that reflects the global motion of the system. The degree of spatial restriction of the local with respect to the global motion is measured by the generalized, model independent order parameter *S*². The value of *S*² ranges from 0 to 1, with *S*² = 0 if the internal motions are isotropic, and *S*² = 1 if the internal motions are completely restricted.^[3]

The fitting was restricted to frequencies above 6 MHz, as at low magnetic fields the SBM theory fails in describing electron-

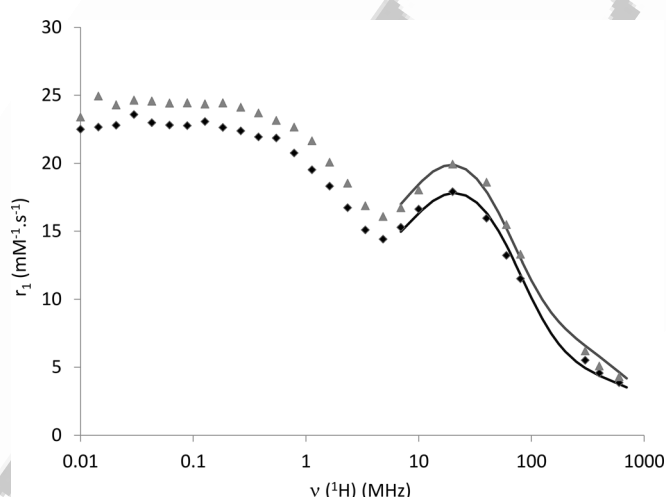


Figure 3. ¹H Nuclear magnetic relaxation dispersion (NMRD) profiles for [DPP-ZnP-GdDOTA]⁻ (1.13 mM, pH 6.6) at 25 °C (▲) and 37 °C (◻) in H₂O. The continuous lines represent the fitted curves. The Gd³⁺ content was determined by ICP-AES measurements.

ic parameters and rotational dynamics of slowly rotating objects. In the fitting procedure, the number of water molecules directly coordinated to Gd^{III} was fixed to 1, and the water exchange rate constant and its activation enthalpy (k_{ex} and ΔH^\ddagger) were fixed to values determined for GdDOTA .^[22] The diffusion constant and its activation energy were also fixed to $D_{\text{GdH}}^{298} = 26 \times 10^{-10} \text{ m}^2 \text{ s}^{-1}$ and $E_{\text{GdH}} = 20 \text{ kJ mol}^{-1}$. The best fit parameters obtained from the analysis of ^1H NMRD data are summarized Table 1 and the Supporting Information, Table S1, and the

Table 1. Best-fit parameters obtained from the fitting of the ^1H NMRD profile to the SBM theory, including the Lipari–Szabo approach for internal flexibility.^[23]

Parameters	[DPP-ZnP-GdDOTA] [−]	[Fe{Gd ₂ bpy(DTTA) ₂ (H ₂ O) ₄ }] ^{4−}
M_w	2448 Da	3744 Da
r_f [mmol L ^{−1} s ^{−1} ; 20 MHz, 25 °C]	19.94	27.03
$q^{[a]}$	1	2
k_{ex}^{298} [10 ⁶ s ^{−1}] ^[a]	4.1	7.4
ΔH^\ddagger [kJ mol ^{−1}] ^[a]	49.8	41.3
E_i [kJ mol ^{−1}]	40 ± 9	–
τ_1^{298} [ps]	245 ± 27	190
E_g [kJ mol ^{−1}]	14 ± 5	–
τ_g^{298} [ps]	2640 ± 200	930
S^2	0.26 ± 0.02	0.6

[a] Fixed during the fitting procedure.

fitted curves are presented in Figure 3. The parameters characterizing electron spin relaxation ($\tau_v = 38 \pm 10$ ps, $\Delta^2 = (0.34 \pm 0.04) \times 10^{19} \text{ s}^{-2}$) are poorly determined by this fit and should not be over-interpreted. In Table 1, we compare our data to those reported for a metallosstar [Fe{Gd₂bpy(DTTA)₂(H₂O)₄}]^{4−} compound which is a discrete molecular contrast agent with six Gd^{III} units conjugated to an iron(II)–tris(bipyridine) complex. Although the metallosstar has a higher molecular weight (3.7 kDa), and a higher hydration number per Gd^{III} (two instead of one for [DPP-ZnP-GdDOTA][−]), we chose this comparison since its rotational dynamics has been also described with the model-free Lipari–Szabo formalism.^[23]

The global and local rotational correlation times obtained for [DPP-ZnP-GdDOTA][−] are longer than those for the metallosstar [Fe{Gd₂bpy(DTTA)₂(H₂O)₄}]^{4−} and are rather similar to the values reported for micellar systems^[17b] (for example, suggesting that the formation of aggregates should be indeed considered to contribute to the high relaxivities). The low value of S^2 shows that the motion of the Gd^{III} -coordinated water proton vector is largely decoupled from the overall motion of the aggregates. One contributing factor to this flexibility is the presence of the alkyl-amide linker between the GdDOTA and the highly rigid porphyrin core. As compared to [Fe{Gd₂bpy(DTTA)₂(H₂O)₄}]^{4−} (Table 1), the relaxivity of our system is lower under similar conditions. This lower relaxivity is related to: 1) its lower hydration number (equal to one instead of two for each of the six Gd centers of {Fe{Gd₂bpy(DTTA)₂(H₂O)₄}]^{4−}), and 2) the increased flexibility of

the Gd^{III} centers in [DPP-ZnP-GdDOTA][−] (lower S^2 value), despite a larger size also reflected in the larger values of the global rotational correlation time, τ_g^{298} (due to the large molecular weight of [DPP-ZnP-GdDOTA][−] and its possible aggregation).

Given the hydrophobic nature of the π -conjugate diketopyrrolopyrrole–zinc(II)porphyrin system, we anticipated a possible interaction of [DPP-ZnP-GdDOTA][−] with serum proteins such as BSA (bovine serum albumin) through hydrophobic interactions.^[24] This interaction would result in a longer τ_R , so an increased relaxivity, as well as a longer circulation time. At 20 MHz and 25 °C, the addition of the physiological concentration of BSA (38 g L^{−1}) yields a relaxivity of 23.94 mmol^{−1} s^{−1}, that is, a circa 20% increase in relaxivity compared to the value in H₂O only (19.94 mmol^{−1} s^{−1}). This indicates the formation of a supramolecular entity between our system and BSA, although it is difficult to know if BSA interacts with the monomeric or the aggregated form of [DPP-ZnP-GdDOTA][−], or both.

Absorption and emission properties: Singlet oxygen production

The theranostic system [DPP-ZnP-GdDOTA][−] was designed for two-photon absorption. However, since the relaxed triplet excited state formed upon two-photon excitation and responsible for the photoreactivity of interest is identical to the one produced by one-photon excitation, we performed a photophysical characterization of the system (absorption, emission, singlet oxygen yield) by a conventional one-photon study. Characteristics such as absorption, and fluorescence quantum yield, are key parameters for the determination of two photon absorption spectra. Moreover, traceability of the photosensitizer inside cells by fluorescence imaging depends on the luminescence efficiency, whereas one- and two-photon phototoxicity induced by singlet oxygen are strictly related to energy transfer from the excited triplet state of the sensitizer to molecular oxygen.

The photophysical characterization of [DPP-ZnP-GdDOTA][−] was performed in three solvents of different polarity: dichloromethane (DCM), dimethyl sulfoxide (DMSO), and water (H₂O).

Absorption spectra obtained in these three solvents are shown in Figure 4. The spectrum in DMSO appears more re-

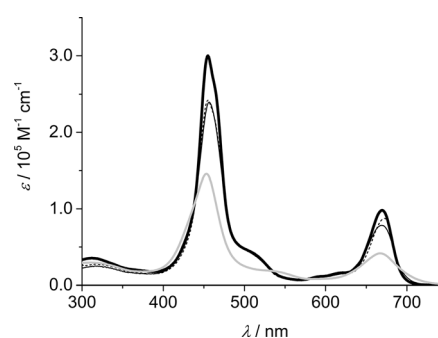


Figure 4. Absorption spectra of [DPP-ZnP-GdDOTA][−] in DCM (black thin), DCM with 1% pyridine (black dashed), DMSO (black thick), and H₂O (gray).

solved than in the other two solvents; in H₂O, in particular, a marked broadening of all bands occurs, very likely ascribable to aggregation phenomena, as also evidenced by relaxometry (see above). In comparison to the precursor DPP-ZnP-TIPS previously characterized,^[11] [DPP-ZnP-GdDOTA][−] displays a bathochromic spectral shift that is possibly due to the extended conjugation introduced by the phenyl group, the shift being more pronounced in DCM than in DMSO (Supporting Information, Figure S15).

Emission spectra recorded at room temperature are displayed in Figure 5 and the relevant luminescence data are collected in Table 2. In DCM and DMSO the typical features of porphyrin fluorescence appear, whereas in H₂O a weak and almost featureless spectrum is observed. In the latter case a very low emission quantum yield and a non-exponential decay, which can be fitted by a bi-exponential function with a good approximation, are observed (Table 2), confirming important aggregation phenomena in this solvent. The fluorescence spectral features of the theranostic system in DCM and DMSO are not affected by the solvent polarity and in both solvents the emission maximum is at ca. 685 nm, overall red-shifted with respect to precursor DPP-ZnP-TIPS.^[11] The emission

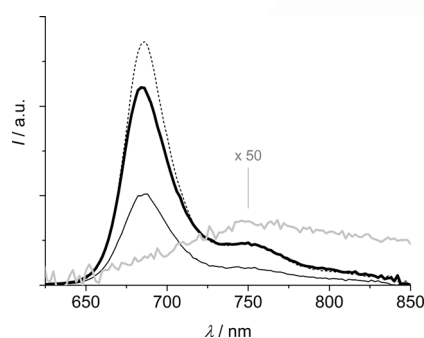


Figure 5. Corrected emission spectra of iso-absorbing solutions of [DPP-ZnP-GdDOTA][−] in DCM (black thin), DCM with 1% pyridine (black dashed), DMSO (black thick), and H₂O (gray). The spectrum in H₂O is multiplied by 50. Excitation is performed at 514 nm ($A_{514} = 0.070$).

decays are single exponentials, with a common value of 0.85 ± 0.1 (Table 2).

The emission quantum yield in DCM is about 2.5 times lower than that in DMSO, which is most likely due to moderate aggregation phenomena. To verify this assumption, the characterization in DCM was also performed in presence of 1% pyridine, which, by axial coordination to the central Zn^{II} ion of the porphyrin, inhibits aggregate formation. Both absorption and emission spectral profiles are almost unaffected by the addition of pyridine (Figure 4 and 5), in contrast to the red shift usually observed for Zn-porphyrin axially complexed by N-ligands, whereas the emission quantum yield recovers the value observed in DMSO (0.14, Table 2), similar to the one measured for precursor DPP-ZnP-TIPS in both solvents (0.15).

Singlet oxygen quantum yield determinations were performed by direct measurement of singlet oxygen phosphorescence in DCM and D₂O and by an indirect method in DMSO. In fact, the poor luminescence properties of singlet oxygen in the latter solvent preclude direct phosphorescence determination.^[25] In DCM, ϕ_{Δ} is of the order of 0.24 with almost no dependence on the concentration of the solution (Table 2 and Figure 6). The addition of pyridine increases this value, and

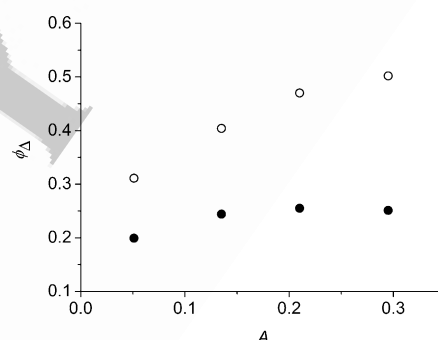


Figure 6. Singlet oxygen production quantum yield of [DPP-ZnP-GdDOTA][−] in DCM (●) and in DCM with 1% pyridine (○) as a function of absorbance at 442 nm.

Table 2. Luminescence data at room temperature. ^[a]					
		λ_{max} [nm] ^[b]	ϕ_{F} ^[c]	τ [ns] ^[d]	ϕ_{Δ} ^[e]
[DPP-ZnP-GdDOTA] [−]	DCM	686, 750 (686, 750)	0.057 (0.14)	0.84 (0.90)	0.24 ± 0.03 (0.42 ± 0.08)
	DMSO	684, 750	0.14	0.86	0.68
	H ₂ O	762	2.2×10^{-3}	0.41 [60 %]; 1.10 [40 %]	— ^[f]
DPP-ZnP-TIPS	DCM	658, 724 ^[g]	0.15 ^[g]	1.06 ^[g]	0.58 ^[g]
	DMSO	672, 734 ^[g]	0.15 ^[g]	1.00 ^[g]	0.54 ^[h]

[a] In round brackets values obtained with 1% pyridine. [b] From corrected emission spectra. [c] Fluorescence quantum yields, measured with reference to TPP (tetraphenylporphyrin) in aerated toluene as a standard. [d] Fluorescence lifetimes, excitation at 560 nm. [e] Singlet oxygen production quantum yields; see the Experimental Section for details. [f] In D₂O, below detection limit. [g] From Ref. [11]. [h] Measured with an indirect method using DPBF as singlet oxygen trap (unpublished results).

a concentration-dependent behavior is observed (Figure 6). The higher value of singlet oxygen quantum yield (mean value: 0.42) can be ascribed to a disaggregation effect induced by pyridine. Nevertheless, this value is also affected by the axial pyridine bond to the central Zn ion that changes the photophysical parameters of the porphyrin. In D₂O, no singlet oxygen signal was observed from [DPP-ZnP-GdDOTA][−], which is most likely due to the aggregation phenomena favoring annihilation processes, lowering the singlet oxygen quantum yield below our experimental detection limit, around 0.1 in these conditions. In DMSO the singlet oxygen quantum yield was determined by using 1,3-diphenylisobenzofuran (DPBF) as a singlet oxygen trap with reference to Zn-phthalocyanine (ZnPc, $\phi_{\Delta} = 0.67$)^[26] (see Experimental Section for details). Figure 7a shows the evolution of the absorption spectrum of a mixture of [DPP-ZnP-GdDOTA][−] and DPBF upon irradiation at 672 nm. Subtraction of the constant contribution of [DPP-ZnP-GdDOTA][−], not experiencing photodegradation, allows the vis-

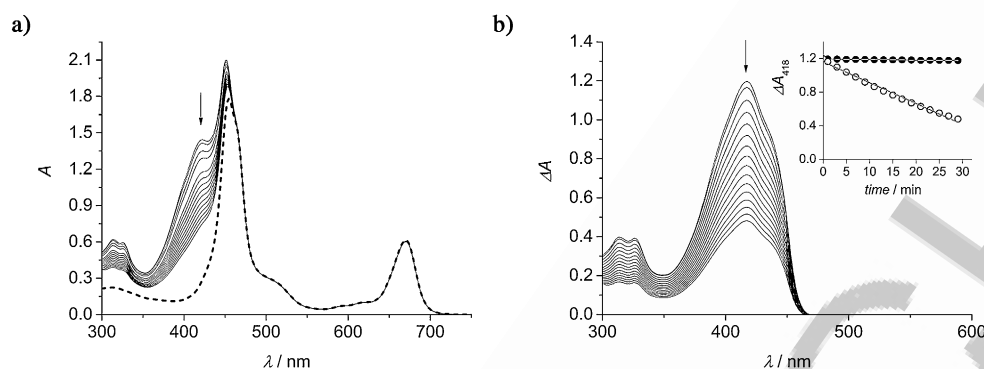


Figure 7. a) Absorption spectra of a DMSO solution containing $[\text{DPP-ZnP-GdDOTA}]^-$ ($7.8 \times 10^{-6} \text{ M}$, ----) and DPBF ($5.2 \times 10^{-5} \text{ M}$) upon irradiation at 672 nm (0–30 min). b) The same spectra as (a) subtracted by the contribution of $[\text{DPP-ZnP-GdDOTA}]^-$. Inset: the value of DPBF absorbance at 418 nm as a function of irradiation time (○; values for the same experiment in the presence of NaN_3 $5.0 \times 10^{-2} \text{ M}$ are shown as ●).

ualization of the consumption of DPBF as a function of the irradiation time (Figure 7b). Addition of NaN_3 to the mixture, a known singlet oxygen quencher, leads to invariance of DPBF absorbance under the same irradiation conditions (Figure 7b inset). By comparison with the degradation rate measured upon irradiation of the standard ZnPc (Supporting Information, Figure S16 and S17) and taking into consideration the intensity of absorption at the excitation wavelength of both the sample and the standard, the ϕ_{Δ} value for $[\text{DPP-ZnP-GdDOTA}]^-$ in DMSO is calculated as 0.68 (Table 2). This value is significantly higher than that measured for DPP-ZnP-TIPS in DMSO ($\phi_{\Delta} = 0.54$, Table 2), showing that the proximity of the Gd^{III} complex has a positive role in increasing the intersystem-crossing yield and hence the triplet yield of the photosensitizer.

$[\text{DPP-ZnP-GdDOTA}]^-$ was found to be thermally and photo-physically stable in the explored solvents and under the employed experimental conditions.

Two-photon excitation spectra

TPA properties were investigated by means of the two-photon induced fluorescence method as described previously.^[11] TPA was studied in DCM containing 1% pyridine to avoid aggregation and in DMSO. The low values of $[\text{DPP-ZnP-GdDOTA}]^-$ fluorescence quantum yield in water precluded the determination of σ_2 in this solvent. Figure 8 shows the two-photon excitation spectra of $[\text{DPP-ZnP-GdDOTA}]^-$ in DCM with 1% pyridine and in DMSO. This agent shows an interesting two-band pattern in the 800–950 nm range with two maxima, one in the 800–840 nm range ($\sigma_2 \approx 750 \text{ GM}$) and one in the 910–940 nm range ($\sigma_2 \approx 1000 \text{ GM}$). The second band is slightly red-shifted from DCM to DMSO, but the TPA intensity is similar in both solvents. Compared to DPP-ZnP-TIPS, the parent molecule without the contrast agent, σ_2 values in DCM are similar, whereas in DMSO, the values are slightly higher. Combined to high singlet oxygen generation quantum yield, these values yield to interesting two-photon singlet oxygen action cross-section $\sigma_2 \cdot \phi_{\Delta}$ (in the range 910–940 nm) of 680 and 460 GM in DMSO and DCM (1% pyridine), respectively.

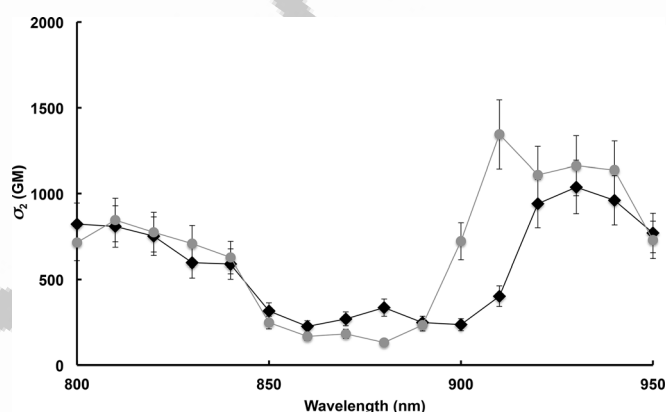


Figure 8. Two-photon excitation spectra of $[\text{DPP-ZnP-GdDOTA}]^-$ in DCM containing 1% pyridine (●) and in DMSO (◆).

Cell behavior

The cellular penetration of $[\text{DPP-ZnP-GdDOTA}]^-$ was studied by confocal microscopy. The presence of the gadolinium complex slows down the cell penetration as compared to DPP-ZnP-TIPS, and the maximum fluorescence signal obtained after incubation of HeLa cells with a $1 \mu\text{M}$ solution of the sensitizer was detected after 24 h instead of 2 h. After 24 h incubation, two-photon excited images (Figure 9) were also registered. The brightness of this system in cells is lower than the one of the parent molecule, indeed the laser power used to acquire contrasted images was higher than for DPP-ZnP-TIPS both in confocal and two-photon excited microscopy.

The dark cytotoxicity of $[\text{DPP-ZnP-GdDOTA}]^-$ was studied by MTT (3-(4,5-dimethylthiazol-2-yl)-2,5-diphenyl tetrazolium bromide) test. A moderate dark toxicity was detected below $2 \mu\text{M}$ after 28 h incubation with the sensitizer (Figure 10).

One-photon phototoxicity

Phototoxicity of $[\text{DPP-ZnP-GdDOTA}]^-$ was investigated using a homemade LED Irradiation apparatus as described by Anderson et al.^[6f] After 24 h incubation with $1 \mu\text{M}$ $[\text{DPP-ZnP-GdDOTA}]^-$ in DMEM containing 1% DMSO, the cells were irra-

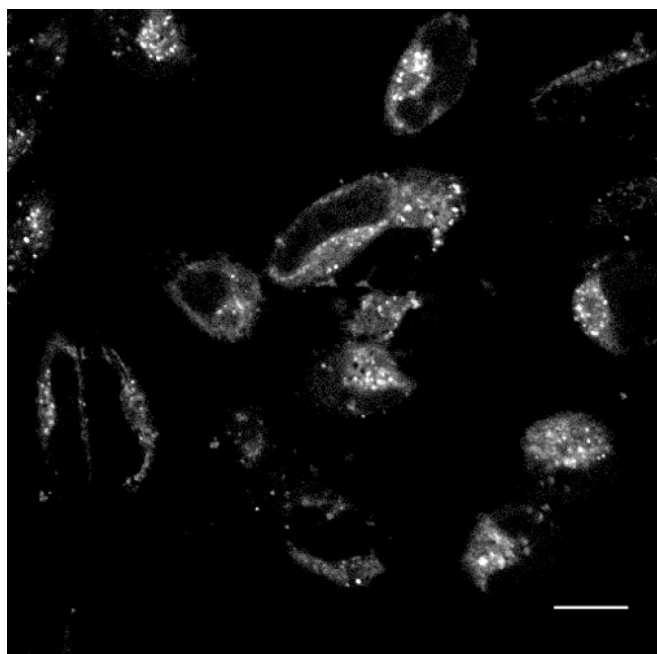


Figure 9. Two-photon excited microscopy image of HeLa cells incubated with 1 μM of [DPP-ZnP-GdDOTA] $^-$ for 24 h ($\lambda_{\text{ex}}=920$ nm, laser power = 10 mW, scale bar = 25 μm).

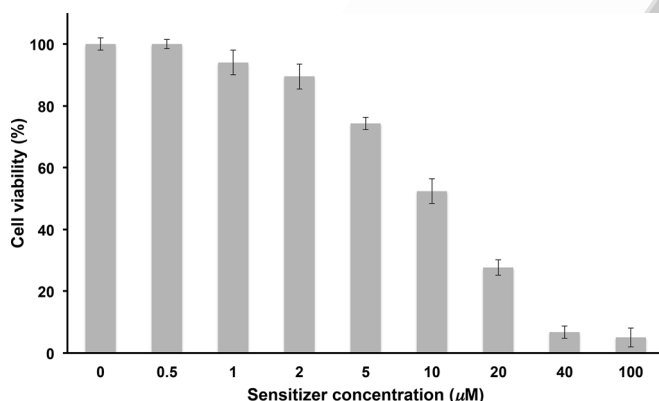


Figure 10. Evaluation of the cytotoxicity of [DPP-ZnP-GdDOTA] $^-$ after 28 h incubation on HeLa cell cultures.

diated one hour ($\lambda_{\text{ex}}=660$ nm, $P=1.7\text{--}4.2$ mW/cm 2). The cell viability was assessed 5 h after irradiation using the MTT assay (Figure 11).

Non-irradiated cells showed a similar toxicity to the one observed for the dark toxicity test. After one-hour irradiation with an irradiance of 4.2 mW/cm 2 , 70% of cell death was detected, even with a low concentration of the sensitizer (1 μM , compared to 10 μM classically used). Irradiations with different powers allowed us to determine the LD $_{50}$ (light dose) of [DPP-ZnP-GdDOTA] $^-$, which was equal to 9 J cm $^{-2}$.

Two-photon phototoxicity

Preliminary two-photon induced cell phototoxicity behavior was explored with 1 μM [DPP-ZnP-GdDOTA] $^-$ as described pre-

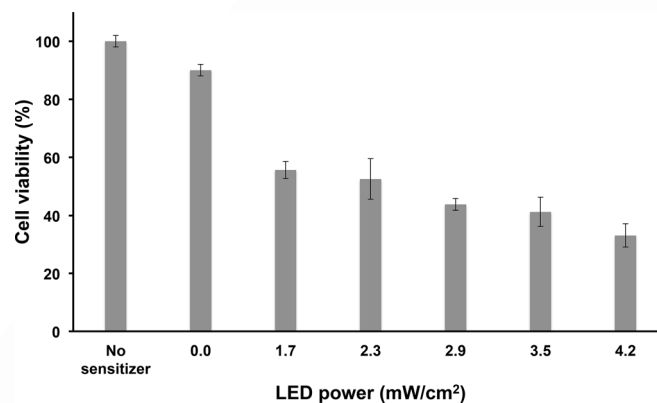


Figure 11. One-photon phototoxicity assay on HeLa cells of [DPP-ZnP-GdDOTA] $^-$ at 1 μM concentration after one hour of irradiation at $\lambda_{\text{ex}}=660$ nm.

viously.^[10a-e] Briefly, 250 \times 250 μm area of a HeLa cell culture was incubated 24 h with [DPP-ZnP-GdDOTA] $^-$ and then irradiated under a TP microscope ($\lambda_{\text{ex}}=930$ nm, $P=8$ mW, 300 scans at 400 Hz, pixel dwell time of 1.4 μs). The cell viability was assessed 4 h after irradiation by means of a double coloration with Hoechst (all cells staining) and Cytos orange (compromised membrane cells) nuclear stains. The irradiation led to about 50% of cell death, whereas the irradiation of a similar cell area not incubated with the sensitizer did not induce significant cell death (2–5% of dead cells). Since non-irradiated zones presented an average cell death of 20%, consistent with the dark toxicity measured with the MTT test, a moderate two-photon phototoxicity of 30% can be inferred (Supporting Information, Figure S18 and S19).

Conclusion

A potential theranostic molecule that associates for the first time a two-photon photosensitizer for PDT with a GdDOTA-based MRI contrast agent was synthesized. The new conjugate [DPP-ZnP-GdDOTA] $^-$ and the Y $^{\text{III}}$ -complexed analogue [DPP-ZnP-YDOTA] $^-$ were obtained in good yield, high purity and were fully characterized. [DPP-ZnP-GdDOTA] $^-$ exhibits a high longitudinal water proton relaxivity, r_1 of 19.94 mm $^{-1}$ s $^{-1}$ at 20 MHz, 25 $^{\circ}\text{C}$ in water and this value is further increased to 23.94 mm $^{-1}$ s $^{-1}$ in the presence of BSA, demonstrating its potential as an efficient contrast agent for in vivo MRI applications. The new molecule has a high two-photon cross section around 1000 GM in DCM (1% pyridine) and DMSO in the 910–940 nm range, corresponding to the therapeutic window. The singlet oxygen generation is high in DMSO and more limited in DCM, where aggregation phenomena occur. Concerning biological applications, the molecule is robust, penetrates in cells and presents low dark toxicity. Preliminary PDT experiments on HeLa cancer cells are promising; the conjugate demonstrates high one-photon and moderate two-photon phototoxicity. Finally, the present system also validates the concept of using a therapeutic agent, here the diketopyrrolopyrrole-zinc(II)porphyrin conjugate, as a vector to convey an imaging

probe of high relaxivity inside cells, in contrast to extracellular agents of clinical use, such as GdDOTA. Such theranostic agents are promising to expand MRI towards novel molecular imaging applications and to perform more efficient PDT treatments.

Experimental Section

General information

All chemicals were of the best commercially available grade and used without further purification. Tetrahydrofuran was dried using a dry solvent station GT S100. Dry chloroform was obtained by distillation over CaH_2 under nitrogen. Triethylamine (Et_3N , 99%), and anhydrous dimethyl sulfoxide (DMSO, 99.7%) were purchased from Aldrich Chemicals (France). Analytical thin-layer chromatography (TLC) was carried out on Merck aluminum backed silica gel 60 F254 plates and visualization when required was achieved using UV light. Precoated plates (PLC Silica gel 60 F₂₅₄, 2 mm) were used for preparative thin-layer chromatography. Column chromatography was carried out on silica (Fluka 60, 70–230 mesh). Size-exclusion chromatography was carried out using Bio-Beads S-X1, 200–400 mesh (Bio-Rad). NMR spectra were recorded at the ambient probe temperature using Bruker AVANCE 300, 400 or 500 spectrometers. Chemical shifts are quoted as parts per million (ppm) relative to the residual peak of solvent and coupling constants (J) are quoted in Hertz (Hz). Where assignments of ^1H NMR spectra are given, they were unambiguously established via COSY, HSQC, HMBC and ROESY experiments. In the assignments, the chemical shift (in ppm) is given first, followed, in brackets, by the multiplicity of the signal (s singlet, d doublet, t triplet, m multiplet, br s broad signal), the number of protons implied, the value of the coupling constants in Hertz if applicable, and finally the assignment. UV/Vis spectra were recorded on a UVKON XL spectrophotometer. Mass spectra were obtained by using a Bruker MicroTOF spectrometer (ES-MS). ICP-AES was performed by emission spectrometry with a Vista AX CCD Simultaneous ICP-AES Varian spectrophotometer.

Compounds *tert*-butoxycarbonyl (Boc)-protected 3-iodobenzylamine (I-Ph-NHBoc),^[13] $\text{Na}_2[\text{GdDOTAGA}]$,^[12] and $\text{Na}_2[\text{YDOTAGA}]$ ^[12] were prepared according to previous reports.

Synthesis of DPP-ZnP-NHBoc

A solution of TBAF (25 mg, 79 μmol) in dry THF (1 mL) was added to a degassed solution of DPP-ZnP-TIPS (147 mg, 79 μmol) in dry THF (24 mL) under argon. The reaction mixture was stirred at room temperature for 20 min and then anhydrous calcium chloride (87 mg, 0.786 mmol) was added. The solvent was evaporated and the crude was submitted to a silica gel column chromatography (DCM/MeOH 96:4). Due to its instability, the deprotected compound DPP-ZnP-H obtained as a brown-green solid was rapidly used for the next reaction.

DPP-ZnP-H (65 mg, 20 μmol), $[\text{Pd}_2(\text{dba})_3]$ (1.7 mg, 2 μmol), CuI (0.5 mg, 2.7 μmol), PPh_3 (2.5 mg, 9.5 μmol), and I-Ph-NHBoc (19 mg, 57 μmol) were dried under vacuum for 1 hour at 45 °C. A solution of dry THF (2 mL) and Et_3N (1 mL) degassed by four freeze-thaw cycles was transferred by cannula to the solids placed under argon. The resulting mixture was stirred at 50 °C for 2 h. The solvents were evaporated and the product was purified by silica gel column chromatography (DCM/pyridine 1%/MeOH 1 to 2%) followed by size-exclusion column chromatography (Bio-Beads S-X1) with DCM. DPP-ZnP-NHBoc was obtained as a brown-green solid in 42% yield (63 mg).

^1H NMR (300 MHz, CDCl_3 + 1% pyridine, 298 K): δ = 1.50 (s, 9H, H_{10}), 3.30 (s, 12H, H_1), 3.33 (s, 3H, H_{25}), 3.39 (s, 3H, H_{20}), 3.44–3.50 (m, 10H, H_{24} , H_2), 3.55–3.57 (m, 4H, H_{23} , H_{19}), 3.60–3.63 (m, 10H, H_3 , H_{18}), 3.66–3.70 (m, 8H, H_4), 3.74–3.79 (m, 10H, H_{22} , H_5), 3.82–3.85 (m, 2H, H_{17}), 3.92–3.95 (m, 8H, H_6), 3.98–4.02 (m, 2H, H_{21}), 4.04–4.08 (m, 2H, H_{16}), 4.29–4.33 (m, 8H, H_7), 4.42 (d, J = 5.5 Hz, 2H, H_8), 5.20 (br s, 1H, H_9), 6.93 (t, J = 2.1 Hz, 2H, p), 7.36 (d, J = 2.2 Hz, 4H, o), 7.45 (d, J = 8.2 Hz, 2H, o'), 7.51–7.53 (m, 3H, mp, pp), 7.96 (d, J = 8.3 Hz, 2H, m'), 7.98–8.01 (m, 2H, op), 8.13 (d, J = 8.5 Hz, 2H, o'), 8.23 (d, J = 8.4 Hz, 2H, m'), 8.91 (d, J = 4.6 Hz, 2H, py_2 or py_3), 8.94 (d, J = 4.6 Hz, 2H, py_2 or py_3), 9.66 (d, J = 4.6 Hz, 2H, py_1 or py_4), 9.67 ppm (d, J = 4.6 Hz, 2H, py_1 or py_4).

^{13}C NMR (125 MHz, CDCl_3 + 1% pyridine, 298 K): δ = 28.53, 42.12, 42.48, 59.04, 59.11, 59.20, 67.89, 68.97, 69.13, 69.92, 70.54, 70.63, 70.74, 70.95, 71.91, 71.97, 93.39, 96.07, 96.23, 96.71, 100.09, 101.07, 101.45, 109.90, 110.15, 114.88, 122.47, 123.31, 127.36, 127.45, 127.82, 128.10, 128.89, 129.42, 129.74, 130.56, 130.80, 131.28, 131.73, 131.83, 132.55, 132.75, 139.51, 144.54, 148.41, 149.29, 149.82, 149.93, 152.04, 152.21, 157.09, 157.94, 163.03, 163.13 ppm.

HR ES-MS: m/z (%) 981.8761 (100) $[\text{M} + 2\text{Na}]^{2+}/2$ (calcd 981.8799 for $[\text{C}_{104}\text{H}_{121}\text{N}_7\text{O}_{24}\text{ZnNa}_2]^{2+}/2$).

Synthesis of DPP-ZnP-NH₂

Compound DPP-ZnP-NHBoc (63 mg, 33 μmol) was dissolved in dry DCM (7 mL). The resulting mixture was cooled to 0 °C before CF_3COOH (0.5 mL) was added dropwise. After 2 h at room temperature, the organic layer was washed with water (7 mL) and aqueous saturated NaHCO_3 (10 mL). The organic layer was dried over Na_2SO_4 , filtered and evaporated. The crude product was dissolved in dry CHCl_3 (20 mL) and a solution of $\text{Zn}(\text{OAc})_2 \cdot 2\text{H}_2\text{O}$ (11 mg, 49 μmol) in MeOH (2 mL) was added dropwise. The resulting mixture was stirred at 50 °C for 3 h. The solvents were evaporated. DCM (10 mL) was added and the solution was washed twice with brine (2 × 10 mL) then with water (10 mL). The organic layer was dried over Na_2SO_4 , filtered and evaporated to dryness. DPP-ZnP-NH₂ was obtained as a brown-green solid in 99% yield (59 mg).

UV/Vis (DCM): λ_{max} (log ϵ) = 458 (5.26), 514 sh, 592 sh, 683 nm (4.88).

^1H NMR (500 MHz, CDCl_3 + 1% pyridine, 298 K): δ = 3.30 (s, 12H, H_1), 3.33 (s, 3H, H_{25}), 3.39 (s, 3H, H_{20}), 3.45–3.49 (m, 10H, H_2 , H_{24}), 3.51–3.53 (m, 2H, H_{19}), 3.54–3.56 (m, 2H, H_{23}), 3.59–3.62 (m, 10H, H_{18} , H_3), 3.67–3.69 (m, 8H, H_4), 3.76–3.78 (m, 12H, H_8 , H_5 , H_{22}), 3.82–3.85 (m, 2H, H_{17}), 3.92–3.94 (m, 8H, H_6), 3.99–4.01 (m, 2H, H_{21}), 4.05–4.07 (m, 2H, H_{16}), 4.30–4.32 (m, 8H, H_7), 6.93 (br s, 2H, p), 7.36–7.38 (m, 6H, o, m'), 7.50–7.53 (m, 3H, mp, pp), 7.94 (d, J = 7.9 Hz, 2H, o'), 7.99–8.00 (m, 2H, op), 8.13 (d, J = 8.2 Hz, 2H, o'), 8.23 (d, J = 8.2 Hz, 2H, m'), 8.91 (d, J = 4.4 Hz, 2H, py_2 or py_3), 8.94 (d, J = 4.4 Hz, 2H, py_2 or py_3), 9.66 (d, J = 4.4 Hz, 2H, py_1 or py_4), 9.67 ppm (d, J = 4.4 Hz, 2H, py_1 or py_4).

^{13}C NMR (125 MHz, CDCl_3 + 1% pyridine, 298 K): δ = 42.08, 42.44, 46.12, 59.06, 59.13, 59.23, 67.81, 68.93, 69.10, 69.90, 70.51, 70.60, 70.71, 70.92, 71.88, 71.93, 93.14, 96.00, 96.34, 96.71, 100.00, 100.95, 101.56, 109.84, 110.09, 114.78, 122.42, 122.77, 123.47, 127.34, 127.40, 128.03, 128.89, 129.41, 129.73, 130.53, 130.80, 131.29, 131.73, 131.77, 132.51, 132.74, 143.07, 144.52, 148.42, 149.29, 149.48, 149.76, 149.87, 152.00, 152.18, 157.88, 163.02, 163.13 ppm.

HR ES-MS: m/z (%) 1818.7247 (100) $[\text{M} + \text{H}]^+$ (calcd 1818.7323 for $[\text{C}_{99}\text{H}_{114}\text{N}_7\text{O}_{22}\text{Zn}]^+$).

Synthesis of Na[DPP-ZnP-MDOTA]

A solution of Na₂[MDOTAGA] (12.7 mmol, L⁻¹, 50 μmol, 1.5 equiv) in dry DMSO was stirred under argon at 60 °C for 5 h. TBTU (18 mg, 56 μmol) and DIPEA (18 μL, 102 μmol) were added to the resulting solution. Then DPP-ZnP-NH₂ (59 mg, 33 μmol) previously dissolved in dry DMSO (2 mL) was added dropwise. The reaction mixture was stirred at room temperature overnight. DMSO was evaporated at 60 °C under reduced pressure before water (10 mL) and DCM (10 mL) were added. The organic layer was washed with water and brine. The organic layer was dried over Na₂SO₄, filtered, and evaporated. The product was purified by size-exclusion column chromatography (Bio-Beads S-X1, 18 g) eluted with DCM, followed by a silica prep-TLC (2 mm) eluted with DCM/MeOH/NH₄OH (80:15:5). The product was extracted from silica three times with a mixture of solvents DCM/MeOH/NH₄OH/DMSO (80:15:4:1). Remaining silica was removed by several centrifugations and filtrations. After evaporation of the solvents, the compound was redissolved in DCM (10 mL) and this solution was washed with water (10 mL) and brine (10 mL). The organic layer was dried over Na₂SO₄, filtered, and evaporated. The compound was dried under vacuum.

Characterization of the gadolinium(III) complex Na[DPP-ZnP-GdDOTA]: Brown-yellow solid (42 mg, 52%).

UV/Vis: (DCM): λ_{max} (log ε) = 455 (5.29), 515 sh, 590 sh, 622 sh, 672 nm (4.85).

HR ES-MS: *m/z* (%) 2475.8193 (100) [M-H₂O+2Na]⁺ (calcd 2475.7982 for [C₁₁₈H₁₃₉GdN₁₁O₃₁ZnNa₂]⁺, 100%)

Characterization of the yttrium(III) complex Na[DPP-ZnP-YDOTA]: Brown-yellow solid.

¹H NMR (300 MHz, DMSO, 298 K): δ = 1.71–1.92 (m, 2H, H₁₀), 2.11–2.92 (m, 25H, DOTA), 3.19 (s, 12H, H₁), 3.20 (s, 3H, H₂₅), 3.25 (s, 3H, H₂₀), 3.38–3.66 (m, 44H, OCH₂), 3.85 (m, 8H, H₆), 3.92 (m, 2H, H₂₁), 3.99 (m, 2H, H₁₆), 4.34 (m, 8H, H₇), 4.35–4.49 (m, 2H, H₈), 7.04 (m, 2H, p), 7.35 (br s, 4H, o), 7.51 (d, 2H, J = 8.1 Hz, m''), 7.62 (m, 3H, mp, pp), 7.97 (m, 2H, op), 8.09 (d, J = 8.1 Hz, 2H, o'), 8.22 (d, J = 8.1 Hz, 2H, o'), 8.31 (d, J = 8.1 Hz, 2H, m'), 8.53 (br s, J = 6.5 Hz, 1H, H₉), 8.91 (d, J = 4.7 Hz, 2H, py2 or py3), 8.93 (d, J = 4.7 Hz, 2H, py2 or py3), 9.71 (d, J = 4.5 Hz, 2H, py1 or py4), 9.76 ppm (d, J = 4.5 Hz, 2H, py1 or py4).

HR ES-MS: *m/z* 2406.7977 [M-H₂O+2Na]⁺ (calcd 2406.7806 for [C₁₁₈H₁₃₉YN₁₁O₃₁ZnNa₂]⁺, 100%)

Spectroscopy and photophysics

DCM and DMSO were of spectroscopic grade from Merck and Carlo Erba, respectively. Tri-distilled (Millipore Milli-Q) water and deuterated water (D₂O) from VWR Chemicals were used. 1,3-diphenylisobenzofuran (DPBF), Zn-phthalocyanine (ZnPc), pyridine, and sodium azide (NaN₃) were from Aldrich.

Absorption spectra were recorded with a PerkinElmer Lambda 650 UV/Vis and with a Lambda 9 UV/Vis-NIR spectrophotometers. Emission spectra were collected with an Edinburgh FLS920 fluorimeter equipped with a Peltier-cooled Hamamatsu R928 PMT (200–850 nm), and corrected for the wavelength dependent phototube response. The fluorescence quantum yields were determined with reference to TPP (tetraphenylporphyrin) in aerated toluene as a standard (φ_{fl} = 0.11).^[27] Fluorescence lifetimes were measured with an IBH time-correlated single photon counting apparatus with excitation both at 465 nm and 560 nm. The analysis of the luminescence decay profiles against time was accomplished with the DAS6 Decay Analysis Software provided by the manufacturer. Estimated errors are 10% on exponential lifetimes, 20% on quantum yields,

20% on molar absorption coefficients and 3 nm on emission and absorption peaks.

Singlet oxygen production quantum yields in DCM and D₂O were measured with reference to Rose Bengal bis(triethylammonium)salt φ_Δ = 0.48 in DCM,^[28] and to 5,10,15,20-tetrakis(4-sulphonatophenyl)porphyrin (TPPS₄) (φ_Δ = 0.64 in D₂O),^[29] respectively, by comparing the intensity of singlet oxygen phosphorescence spectra measured with a FLS920 spectrofluorimeter (Edinburgh) equipped with a Hamamatsu R5509–72 supercooled photomultiplier tube at 193 K and a TM300 emission monochromator with a grating blazed at 1000 nm. Excitation at 442 nm was performed with a Kimmon Koha Co., Ltd. HeCd laser (the power was reduced to ca. 7 mW to avoid annihilation effects).

Singlet oxygen production quantum yield in DMSO was measured with a comparative method using DPBF as a singlet oxygen trap, which is oxidized by singlet oxygen and its degradation can be monitored by the decrease of its absorbance at 418 nm.^[30] ZnPc was used as a standard (φ_Δ = 0.67).^[26] Solutions of the standard or of the Gd complex containing DPBF 5.2 × 10⁻⁵ M, prepared in the dark, were irradiated at 672 nm (A₆₇₂ = 0.6) by using an irradiation set-up composed by a 150 W xenon lamp (LOT) and a Omni-λ 150 monochromator (Zolix), under continuous stirring. The light intensity was 12 mWcm⁻². The singlet oxygen quantum yield of the sample (φ_Δ) were determined by using Equation (1):

$$\phi_{\Delta} = \phi_{\Delta}^{\text{std}} \frac{R \cdot I_{\text{abs}}^{\text{std}}}{R^{\text{std}} \cdot I_{\text{abs}}} \quad (1)$$

where *R* and *R*^{std} are the DPBF degradation rates for the sample and the standard, respectively, and *I*_{abs} is the intensity of absorption at the excitation wavelength calculated as described in reference.^[30] NaN₃ was used at the concentration of 5.0 × 10⁻² M to efficiently quench the produced singlet oxygen.^[31] Small changes in the absorption spectra of both sample and standard were observed upon the addition of NaN₃.

Two-photon photophysical properties

The TPA cross-section spectra were obtained by up-conversion fluorescence measurements^[32] using an Insight Spectra-Physics (680 nm/1300 nm) femtosecond laser. The excitation beam is collimated over the cell length (10 mm). The fluorescence, collected at 90° of the excitation beam, was focused into an optical fiber connected to a spectrometer. The incident beam intensity was adjusted to ensure an intensity-squared dependence of the fluorescence over the whole spectral range. Calibration of the spectra was performed by comparison with the published 800–950 nm Rhodamine B two-photon absorption spectrum.^[33] Below 800 nm, a significant contribution from one-photon absorption was noticed by a non-quadratic dependency dependence of the emitted fluorescence vs the laser power and points below this wavelength were discarded.

Cell culture

HeLa cells were cultured in DMEM complete culture medium containing phenol red. They were seeded and maintained in LabTek (Lab-Tek II) or Ibidi (μ-Dish 35 mm Grid-500) culture flasks or petri dishes for two-photon microscopy. The Ibidi Grid 500 petri dish presents a grid with 500 × 500 μm on the glass bottom allowing an easy localization of the irradiation zones in TP-PDT experiments. MTT toxicity test were performed in tetraplicates with extempor-

neous solutions of 3-(4,5-dimethyl-2-thiazolyl)-2,5-diphenyl-2H-tetrazolium bromide.


One-photon phototoxicity tests

One-photon phototoxicity tests were performed, as described previously, using a homemade apparatus^[6f] using 5 mm 660 nm Lite-on LED (Mouser electronics ref. 859-LTL-353CKR-H3) adapted for black Corning 96-well special optics plates. Cells were cultured 2 days in these 96-well plates and incubated with 1 μM solution of Na[DPP-ZnP-GdDOTA] in complete DMEM medium containing 1% DMSO for 24 h. The plates were irradiated 1 hour and the light intensity was measured with a power-meter. The cell viability was estimated 5 h after irradiation as described in the cell culture paragraph.

Two-photon imaging and two-photon photodynamic therapy

Two-photon microscopy studies were performed on a Leica SP8 inverted microscope with x 63 λBlue HCS plan apo objective. A Coherent Chameleon Ultra 2 laser was used for irradiation with 150 fs pulses with a repetition rate of 80 MHz at $\lambda_{\text{ex}} = 910$ nm. A region of $250 \times 250 \mu\text{m}$ was irradiated (1.4 $\mu\text{s}/\text{pixel}$) with a power of about 5.9 mW at the back pupil of the objective.

HeLa cells were incubated 24–28 h with 1 μM of [DPP-ZnP-GdDOTA][−] in DMEM culture medium containing 1% DMSO.

Before irradiation, a phase contrast image of the  was taken to assess the number of cells before irradiation.

After TP-PDT irradiation, the cells were left 4 h in an incubator. Then, cell viability was determined by staining with Hoechst nuclear stain (a blue fluorescence indicates the nucleus of all cells) combined with Cytos orange. This later allows for detection of cells with compromised cytoplasmic membrane (an orange fluorescence indicating dead cells). Confocal images were obtained with a Leica TSP SPE microscope using two channels, one for Hoescht (ex. 405 nm) and one for CYTOX orange (561 nm). We noticed that dead HeLa cells detached from the glass bottom and were therefore not detected with confocal microscopy.

A control experiment to test the viability of cells under TP irradiation in absence of the sensitizer [DPP-ZnP-GdDOTA][−] (but with 1% DMSO) was performed. It showed that the cell viability was above 95% after 300 scans of irradiation, performed in the same conditions as with [DPP-ZnP-GdDOTA][−].

Relaxometric measurements

Proton NMRD profiles ([DPP-ZnP-GdDOTA][−] = 1.13 mM, pH 6.6 in H₂O, and [DPP-ZnP-GdDOTA][−] = 0.96 mM, pH 6.85 in aqueous NaCl 50 mM) were recorded on a Stelar SMARTTracer Fast Field Cycling relaxometer (0.01–10 MHz) and a Bruker WP80 NMR electromagnet adapted to variable field measurements (20–80 MHz) and controlled by a SMARTTracer PC NMR console. Higher field relaxivities were measured on Bruker AVANCE NMR spectrometers at 300 MHz, 400 MHz, and 600 MHz. The temperature was monitored by a VTC91 temperature control unit and maintained by a gas flow. The temperature was determined by previous calibration with a Pt resistance temperature probe. The longitudinal relaxation rates (1/ T_1) were determined in water and in aqueous NaCl 50 mM. The least-squares fit of the ¹H NMRD data was performed using Visualiseur/Optimiseur^[34] running on a MATLAB 8.3.0 (R2014a) platform. The relaxivity was also measured in the presence of BSA 38 g L^{−1}

for [DPP-ZnP-GdDOTA][−] = 0.23 mM, in H₂O at 298 K and 20 MHz. The exact Gd^{III} ion concentration was determined by ICP-AES analysis after microwave-assisted mineralization.

Acknowledgements

We thank Agnès Pallier for performing relaxivity measurements. The icFRC (<http://www.icfrc.fr>) and Region Alsace are gratefully acknowledged for a fellowship to J.S., and the Ligue contre le Cancer for financial support. We thank warmly E. Leize, C. Perret, and H. Nierengarten for the HR mass-spectrometry determination. The Italian CNR (Project PM.P04.010 “MACOL”), MIUR project PRIN 2010CX2TLM, and MIUR-CNR project Nanomax N-CHEM are gratefully acknowledged.

Keywords: diketopyrrolopyrrole • gadolinium • magnetic resonance imaging • photodynamic therapy • porphyrins • two-photon absorption

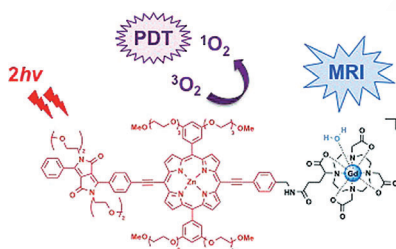
- [1] a) H. Cabral, N. Nishiyama, K. Kataoka, *Acc. Chem. Res.* **2011**, *44*, 999–1008; b) T. Lammers, S. Aime, W. E. Hennink, G. Storm, F. Kiessling, *Acc. Chem. Res.* **2011**, *44*, 1029–1038.
- [2] P. Caravan, J. J. Ellison, T. J. McMurphy, R. B. Lauffer, *Chem. Rev.* **1999**, *99*, 2293–2352.
- [3] E. Tóth, L. Helm, A. E. Merbach in *The Chemistry of Contrast Agents in Medical Magnetic Resonance Imaging*, 2nd edn. Wiley and Sons, New York, Relaxivity of Gadolinium(III) Complexes (Chapter 2) **2013**, pp. 25–82.
- [4] E. J. Werner, A. Datta, C. J. Jocher, K. N. Raymond, *Angew. Chem. Int. Ed.* **2008**, *47*, 8568–8580; *Angew. Chem.* **2008**, *120*, 8696–8709.
- [5] a) T. J. Dougherty, C. J. Gomer, B. W. Henderson, G. Jori, D. Kessel, M. Korbekli, J. Moan, Q. Peng, *J. Nat. Cancer Inst.* **1998**, *90*, 889–905; b) C. W. Brian, S. P. Michael, *Phys. Med. Chem.* **2008**, *53*, R61; c) M. Ethirajan, Y. Chen, P. Joshi, R. K. Pandey, *Chem. Soc. Rev.* **2011**, *40*, 340–362.
- [6] a) K. Ogawa, H. Hasegawa, Y. Inaba, Y. Kobuke, H. Inouye, Y. Kanemitsu, E. Kohno, T. Hirano, S.-i. Ogura, I. Okura, *J. Med. Chem.* **2006**, *49*, 2276–2283; b) M. A. Oar, W. R. Dichtel, J. M. Serin, J. M. J. Fréchet, J. E. Rogers, J. E. Slagle, P. A. Fleitz, L.-S. Tan, T. Y. Ohulchanskyy, P. N. Prasad, *Chem. Mater.* **2006**, *18*, 3682–3692; c) M. Khurana, H. A. Collins, A. Karotki, H. L. Anderson, D. T. Cramb, B. C. Wilson, *Photochem. Photobiol.* **2007**, *83*, 1441–1448; d) H. A. Collins, M. Khurana, E. H. Moriyama, A. Mariampillai, E. Dahlstedt, M. Balaz, M. K. Kuimova, M. Drobizhev, X. D. Yang-Victor, D. Phillips, A. Rebane, B. C. Wilson, H. L. Anderson, *Nat. Photonics* **2008**, *2*, 420–424; e) J. R. Starkey, A. K. Rebane, M. A. Drobizhev, F. Meng, A. Gong, A. Elliott, K. McInerney, C. W. Spangler, *Clin. Cancer Res.* **2008**, *14*, 6564–6573; f) E. Dahlstedt, H. A. Collins, M. Balaz, M. K. Kuimova, M. Khurana, B. C. Wilson, D. Phillips, H. L. Anderson, *Org. Biomol. Chem.* **2009**, *7*, 897–904; g) M. Pawlicki, H. A. Collins, R. G. Denning, H. L. Anderson, *Angew. Chem. Int. Ed.* **2009**, *48*, 3244–3266; *Angew. Chem.* **2009**, *121*, 3292–3316.
- [7] J. P. Celli, B. Q. Spring, I. Rizvi, C. L. Evans, K. S. Samkoe, S. Verma, B. W. Pogue, T. Hasan, *Chem. Rev.* **2010**, *110*, 2795–2838.
- [8] M. Montaldi, A. Credi, L. Prodi, M. T. Gandolfi in *Vol. Handbook of Photochemistry*, 3rd ed., CRC Press, Taylor & Francis, Boca Raton, **2006**, p. 620.
- [9] a) G. Li, A. Slansky, M. P. Dobhal, L. N. Goswami, A. Graham, Y. Chen, P. Kanter, R. A. Alberico, J. Sperryak, J. Morgan, R. Mazurchuk, A. Oseroff, Z. Grossman, R. K. Pandey, *Bioconjugate Chem.* **2005**, *16*, 32–42; b) L. N. Goswami, W. H. White, J. A. Sperryak, M. Ethirajan, Y. Chen, J. R. Missert, J. Morgan, R. Mazurchuk, R. K. Pandey, *Bioconjugate Chem.* **2010**, *21*, 816–827; c) J. A. Sperryak, W. H. White, M. Ethirajan, N. J. Patel, L. Goswami, Y. Chen, S. Turowski, J. R. Missert, C. Batt, R. Mazurchuk, R. K. Pandey, *Bioconjugate Chem.* **2010**, *21*, 828–835; d) J. Luo, L.-F. Chen, P. Hu, Z.-N. Chen, *Inorg. Chem.* **2014**, *53*, 4184–4191; e) K. S. Samkoe, A. Chen, I. Rizvi, J. A. O'Hara, J. P. Hoopes, T. Hasan, B. W. Pogue in *Optical*

- Methods for Tumor Treatment and Detection: Mechanisms and Techniques in Photodynamic Therapy XVIII*, Vol. 7164 (Ed.: D. H. Kessel), **2009**, p. 71640D; f) D. Aydın Tekdaş, R. Garifullin, B. Şentürk, Y. Zorlu, U. Gundogdu, E. Atalar, A. B. Tekinay, A. A. Chernonosov, Y. Yerli, F. Dumoulin, M. O. Guler, V. Ahsen, A. G. Gürek, *Photochem. Photobiol.* **2014**, *90*, 1376–1386; g) H. Haroon-Ur-Rashid, M. N. Umar, K. Khan, M. N. Anjum, M. Yaseen, *J. Struct. Chem.* **2014**, *55*, 910–915.
- [10] a) R. Kopelman, Y.-E. Lee Koo, M. Philbert, B. A. Moffat, G. Ramachandra Reddy, P. McConville, D. E. Hall, T. L. Chenevert, M. S. Bhojani, S. M. Buck, A. Rehemtulla, B. D. Ross, *J. Magn. Magn. Mater.* **2005**, *293*, 404–410; b) G. R. Reddy, M. S. Bhojani, P. McConville, J. Moody, B. A. Moffat, D. E. Hall, G. Kim, Y.-E. L. Koo, M. J. Woolliscroft, J. V. Sugai, T. D. Johnson, M. A. Philbert, R. Kopelman, A. Rehemtulla, B. D. Ross, *Clin. Cancer Res.* **2006**, *12*, 6677–6686; c) J. R. McCarthy, F. A. Jaffer, R. Weissleder, *Small* **2006**, *2*, 983–987; d) C.-W. Lai, Y.-H. Wang, C.-H. Lai, M.-J. Yang, C.-Y. Chen, P.-T. Chou, C.-S. Chan, Y. Chi, Y.-C. Chen, J.-K. Hsiao, *Small* **2008**, *4*, 218–224; e) A. Vaidya, Y. Sun, Y. Feng, L. Emerson, E.-K. Jeong, Z.-R. Lu, *Pharm. Res.* **2008**, *25*, 2002–2011; f) X. Liang, X. Li, L. Jing, X. Yue, Z. Dai, *Biomaterials* **2014**, *35*, 6379–6388; g) H.-J. Yoon, T. G. Lim, J.-H. Kim, Y. M. Cho, Y. S. Kim, U. S. Chung, J. H. Kim, B. W. Choi, W.-G. Koh, W.-D. Jang, *Biomacromolecules* **2014**, *15*, 1382–1389.
- [11] J. Schmitt, V. Heitz, A. Sour, F. Bolze, H. Ftouni, J.-F. Nicoud, L. Flamigni, B. Ventura, *Angew. Chem. Int. Ed.* **2015**, *54*, 169–173; *Angew. Chem.* **2015**, *127*, 171–175.
- [12] J. Henig, E. Tóth, J. Engelmann, S. Gottschalk, H. A. Mayer, *Inorg. Chem.* **2010**, *49*, 6124–6138.
- [13] T. Odani, S. Okada, C. Kabuto, T. Kimura, S. Shimada, H. Matsuda, H. Oikawa, A. Matsumoto, H. Nakanishi, *Cryst. Growth Des.* **2009**, *9*, 3481–3487.
- [14] L. Vander Elst, M. Port, I. Raynal, C. Simonot, R. N. Muller, *Eur. J. Inorg. Chem.* **2003**, 2495–2501.
- [15] A. Carné-Sánchez, C. S. Bonnet, I. Imaz, J. Lorenzo, É. Tóth, D. Maspoch, *J. Am. Chem. Soc.* **2013**, *135*, 17711–17714.
- [16] J. W. Fredy, J. Scelle, A. Guenet, E. Morel, S. Adam de Beaumais, M. Ménand, V. Marvaud, C. S. Bonnet, E. Tóth, M. Sollogoub, G. Vives, B. Hasenknopf, *Chem. Eur. J.* **2014**, *20*, 10915–10920.
- [17] a) A. Martins, J.-F. Morfin, C. G. C. Geraldès, É. Tóth, *J. Biol. Inorg. Chem.* **2014**, *19*, 281–295; b) G. Nicolle, É. Tóth, K.-P. Eisenwiener, H. Mäcke, A. Merbach, *J. Biol. Inorg. Chem.* **2002**, *7*, 757–769.
- [18] M. F. Ferreira, J. Gonçalves, B. Mousavi, M. I. M. Prata, S. P. J. Rodrigues, D. Calle, P. Lopez-Larrubia, S. Cerdan, T. B. Rodrigues, P. M. Ferreira, L. Helm, J. A. Martins, C. F. G. C. Geraldès, *Dalton Trans.* **2015**, *44*, 4016–4031.
- [19] R. F. Pasternack, P. R. Huber, P. Boyd, G. Engasser, L. Francesconi, E. Gibbs, P. Fasella, G. Cerio Ventura, L. d. Hinds, *J. Am. Chem. Soc.* **1972**, *94*, 4511–4517.
- [20] a) J. Costa, E. Balogh, V. Turcyr, R. Tripier, M. Le Baccon, F. Chuburu, H. Handel, L. Helm, É. Tóth, A. E. Merbach, *Chem. Eur. J.* **2006**, *12*, 6841–6851; b) M. Regueiro-Figueroa, A. Nonat, G. A. Rolla, D. Esteban-Gómez, A. de Blas, T. Rodríguez-Blas, L. J. Charbonnière, M. Botta, C. Platas-Iglesias, *Chem. Eur. J.* **2013**, *19*, 11696–11706; c) H. Jaccard, P. Miéville, C. Cannizzo, C. Mayer, L. Helm, *J. Biol. Inorg. Chem.* **2014**, *19*, 145–159; d) S. Aime, C. Cabella, S. Colombatto, S. Geninatti Crich, E. Gianolio, F. Maggioni, *J. Mag. Reson. Imaging* **2002**, *16*, 394–406; e) S. Aime, É. Tóth, L. Helm, K. E. Kellar, A. E. Merbach, *Chem. Eur. J.* **1999**, *5*, 1202–1211.
- [21] D. H. Powell, O. M. N. Dhubhghaill, D. Pubanz, L. Helm, Y. S. Lebedev, W. Schlaepfer, A. E. Merbach, *J. Am. Chem. Soc.* **1996**, *118*, 9333–9346.
- [22] J. B. Livramento, A. Sour, A. Borel, A. E. Merbach, É. Tóth, *Chem. Eur. J.* **2006**, *12*, 989–1003.
- [23] S. Aime, M. Botta, M. Fasano and E. Terreno in *The chemistry of contrast agents in medical magnetic resonance imaging*, Vol. Eds.: J. Wiley and Sons), Protein-bound metal chelates, **2001**, pp. 193–242.
- [24] F. Wilkinson, J. G. Brummer, *J. Phys. Chem. Ref. Data* **1981**, *10*, 809–1000.
- [25] A. Ogunsipe, J.-Y. Chen, T. Nyokong, *New J. Chem.* **2004**, *28*, 822–827.
- [26] P. G. Seybold, M. Gouterman, *J. Mol. Spectrosc.* **1969**, *31*, 1–13.
- [27] J. J. M. Lamberts, D. R. Schumacher, D. C. Neckers, *J. Am. Chem. Soc.* **1984**, *106*, 5879–5883.
- [28] C. Tanielian, C. Wolff, M. Esch, *J. Phys. Chem.* **1996**, *100*, 6555–6560.
- [29] I. Seotsanyana-Mokhosi, N. Kuznetsova, T. Nyokong, *J. Photochem. Photobiol. A* **2001**, *140*, 215–222.
- [30] M. J. Moreno, E. Monson, R. G. Reddy, A. Rehemtulla, B. D. Ross, M. Philbert, R. J. Schneider, R. Kopelman, *Sensor Actuat. B Chem.* **2003**, *90*, 82–89; e) S. Aime, É. Tóth, L. Helm, K. E. Kellar, A. E. Merbach, *Chem. Eur. J.* **1999**, *5*, 1202–1211.
- [31] A. Hayek, F. Bolze, C. Bourgogne, P. L. Baldeck, P. Didier, Y. Arntz, Y. Mély, J.-F. Nicoud, *Inorg. Chem.* **2009**, *48*, 9112–9119.
- [32] C. Xu, W. W. Webb, *J. Opt. Soc. Am. B* **1996**, *13*, 481–491.
- [33] F. Yerly in *VISUALISEUR 2.3.5, OPTIMISEUR 2.3.5*, Vol. Lausanne, Switzerland, **1999**.

Received: August 28, 2015
Published online on ■■■ ■■, 0000

FULL PAPER

A bifunctional agent that combines a (diketopyrrolopyrrole)porphyrin component as a two-photon photosensitizer for photodynamic therapy (PDT) with a gadolinium(III) DOTA complex as a magnetic resonance imaging probe was synthesized. Relaxometric, photo-physical, and in cell studies highlight the potential of this molecule as a theranostic agent.



Photodynamic Therapy

J. Schmitt, V. Heitz,* A. Sour, F. Bolze,*
P. Kessler, L. Flamigni, B. Ventura,*
C. S. Bonnet, É. Tóth*

**A Theranostic Agent Combining
a Two-Photon-Absorbing
Photosensitizer for Photodynamic
Therapy and a Gadolinium(III)
Complex for MRI Detection**

Please check that the ORCID identifiers listed below are correct. We encourage all authors to provide an ORCID identifier for each coauthor. ORCID is a registry that provides researchers with a unique digital identifier. Some funding agencies recommend or even require the inclusion of ORCID IDs in all published articles, and authors should consult their funding agency guidelines for details. Registration is easy and free; for further information, see <http://orcid.org/>.

Julie Schmitt
Valérie Heitz
Angélique Sour
Frédéric Bolze
Pascal Kessler
Lucia Flamigni
Barbara Ventura
Célia S. Bonnet
Éva Tóth